Inorganic Chemistry

Article

pubs.acs.org/IC

Cation Exchange in Small ZnS and CdS Molecular Analogues

Swamy Pittala and Kevin R. Kittilstved*

Department of Chemistry, University of Massachusetts Amherst, 122 Lederle GRC, 710 North Pleasant Street, Amherst, Massachusetts 01003, United States

Supporting Information

ABSTRACT: The simplest means of altering the chemistry and electronic structure of any material, from molecular clusters to single crystals, is by the introduction of chemical impurities. We present a systematic study of the cation exchange reaction involving Co^{2+} ions with metal benzenethiolate clusters, $[M_4(SPh)_{10}]^{2-}$ (M = Zn, Cd), yielding diluted magnetic clusters having the general formula $[(M_{1-x}Co_x)_4(SPh)_{10}]^{2-}$. This method allows high concentrations of doping at the molecular level without forming concentrated magnetic clusters such as $[Co_4(SPh)_{10}]^{2-}$. Changes in the electronic structure of the molecular species containing on average <1 Co^{2+} per cluster were observed and characterized by a variety of analytical (high-resolution electrospray mass spectrometry) and spectroscopic techniques (electronic absorption including stopped-flow kinetics, luminescence, and paramagnetic ^1H NMR). The mass spectrometry results strongly suggest that the cation exchange reaction with Co^{2+} is thermodynamically favored for the $[Zn_4(SPh)_{10}]^{2-}$ cluster compared to the $[Cd_4(SPh)_{10}]^{2-}$ clusters at room temperature. The rate of the cation exchange is orders of magnitude faster for the $[Cd_4(SPh)_{10}]^{2-}$ cluster than for $[Zn_4(SPh)_{10}]^{2-}$ and is governed by ligand interconversion processes. This simple room temperature cation exchange into molecular clusters is a model reaction that provides important structural information regarding the effect of Co^{2+} doping on the cluster stability.

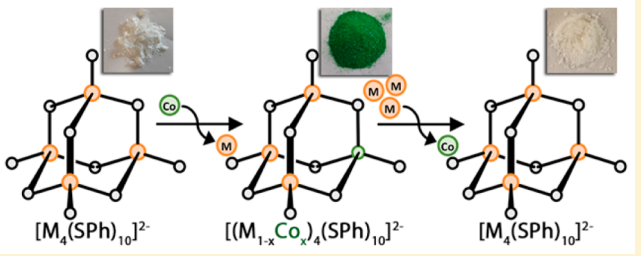

1. INTRODUCTION

Colloidal II−VI semiconductor quantum dots (QDs) have impacted many fields of science and engineering due to their size-tunable chemical and photophysical properties.[1−3] Introduction of paramagnetic metal ions into colloidal semiconductor nanocrystals, also known as diluted magnetic semiconductor QDs (DMS-QDs), exhibit many interesting optical, magnetic, and electronic properties due to the strong exchange interaction (sp−d) between charge carriers of the semiconductor and magnetic ions. The defining feature of the sp−d exchange is the giant Zeeman splitting of charge carriers in the valence and conduction bands, which is maximized when the dopant is at the center of the nanocrystal thus enabling optimum overlap between the wave functions of the dopant ion and the spatially confined exciton.[4−6] Although many reports describe synthetic approaches to doping paramagnetic ions into various QDs,[7−12] the synthesis of colloidal DMS-QDs with controlled and homogeneous dopant distributions remains a challenge.

The first report of successful internal doping of CdSe QDs with Co^{2+} dopants by high-temperature techniques utilized $(NMe_4)_2[Cd_4(SePh)_{10}]$ molecular clusters and $CoCl_2$ as the host and dopant precursors, respectively.[13] The successful doping by this method is in part due to the separation of the nucleation and growth compared to the conventional "hot injection" method to prepare high-quality QDs.[10,14,15] Even though this cluster degradation method led to the successful doping of other novel II−VI colloidal DMS-QDs in addition to Co^{2+}-doped CdSe, confirmation of dopant incorporation into the critical nucleus at the stage of nanocrystal nucleation remains elusive.[6] Furthermore, the general mechanism of dopant incorporation into DMS-QDs remains an active area of research and has recently included the doping of small clusters.[16−21] For instance, Yu et al. achieved a very large splitting of the exciton in Mn^{2+}-doped CdSe quantum nanoribbons ($g_{eff} \sim 600$ at 1.8 K) by controlling the composition of the molecular clusters at nucleation.[22] Successful doping of magnetic ions into discrete "magic-sized" clusters has also been reported for Mn^{2+}:ZnTe.[23] A primary objective of research in this field is to find new synthetic routes to prepare precision-doped DMS-QDs to increase the dopant−exciton overlap. In order to synthesize DMS-QDs with homogeneous dopant distributions throughout the nanocrystal, we need a more thorough understanding of the molecular processes that promote dopant incorporation into the QD at the nucleation stage.

Cation exchange and reversible exchange processes are promising postsynthetic methods to control compositions (or heavily doped) and shape of colloidal nanocrystals due to the excellent morphology retention and rapid reaction rates.[24−26] For example, several groups reported the synthesis of Ag^+-doped CdSe nanocrystals by cation exchange reactions at room temperature.[26,27] However, there are no reports of para-

Received: February 23, 2015
Published: June 3, 2015

DOI: 10.1021/acs.inorgchem.5b00421
Inorg. Chem. 2015, 54, 5757−5767

magnetic transition metal (TM^{2+} = Mn^{2+}, Co^{2+}, and Fe^{2+}) doping of colloidal II−VI nanocrystals using only cation exchange. A fundamental understanding of the kinetic and thermodynamic factors that govern cation exchange at QD surfaces is greatly needed. In this study we focus on using cation exchange reactions to substitute transition metal ions into small molecular analogues of CdS and ZnS nanocrystals. The small number of atoms and high surface area provide more flexibility to the clusters than the nanocrystals, which allows the clusters to accommodate structural deformation during the exchange without changing morphology.

The study of the chemistry and photophysics of tetrameric metal benzenechalcogenolate molecular clusters with the general formula $(NMe_4)_2[M_4(EPh)_{10}]$ (M = Cd, Zn, Fe, and Co; E = S, Se) was initiated over 30 years ago due to their structural similarity to multinuclear clusters in cysteine-rich proteins (metallothionein).[28−33] Recently, these molecular clusters have become attractive model systems for II−VI QDs due to their inherent monodispersity and atomically precise compositions.[34−36] The tetrameric cluster possesses an adamantane-like $[(\mu\text{-SPh})_6M_4]$ core with the M^{2+} sites occupying the corners of a tetrahedron and coordinating with three bridging benzenethiolates. The remaining four benzenthiolate ligands bind each of M^{2+} sites to complete the structure and provide a pseudotetrahedral environment for each M^{2+} ion. We regard these tetrameric molecular clusters in particular as ideal models of the QD surface that will provide insight into the underlying doping mechanism of QDs by studying the dynamics of the cation exchange reactions. In addition, recent interest in these and similar Co^{2+}-containing compounds was generated by the demonstration of slow magnetic relaxation of the magnetization in mononuclear $(Ph_4P)_2[Co(SPh)_4]$, due to its large and negative axial component to the zero-field splitting of the $^4A_2$ ground state.[37,38] Similar structural distortions around the Co^{2+} ion in other complexes appears to be a general design motif for mononuclear magnetic systems based on pseudotetrahedral $[CoS_4]^{2-}$ complexes.[39,40] However, the large single-ion anisotropy is lost in the tetrameric $[Co_4(SPh)_{10}]^{2-}$ clusters, which possesses only antiferromagnetic coupling between Co^{2+} ions.

Herein we present a detailed and systematic experimental study of Co^{2+} exchange reactions with $(NMe_4)_2[Zn_4(SPh)_{10}]$ and $(NMe_4)_2[Cd_4(SPh)_{10}]$ molecular clusters using electronic absorption, luminescence, and ^1H NMR spectroscopies to confirm the speciation of the dopant ions in the molecular clusters. Variable-temperature NMR spectroscopy and stopped-flow kinetics measurements were performed to determine cation exchange rates and cluster dynamics at equilibrium. Ligand-field and charge transfer electronic transitions are observed in the absorption spectra that are unique to the diluted molecular clusters. To complement the spectroscopic studies, we also performed high-resolution electrospray ionization mass spectrometry (ESI-MS) to confirm and quantify the relative substitution yields in the clusters with different compositions. Our results unambiguously confirm the successful substitution of Co^{2+} into both $[Zn_4(SPh)_{10}]^{2-}$ and $[Cd_4(SPh)_{10}]^{-}$ clusters. Furthermore, we present evidence that Co^{2+} exchange into $[Zn_4(SPh)_{10}]^{2-}$ clusters is thermodynamically favored compared to the $[Cd_4(SPh)_{10}]^{2-}$ clusters that have a large mismatch in covalent radii. However, the rate of cation exchange is primarily governed by ligand interconversion rates (bridging $PhS^- \leftrightarrow$ terminal PhS^-) in solution and are much faster for the $[Cd_4(SPh)_{10}]^{-}$ clusters as deduced from the temperature dependence of the NMR spectra and confirmed by stopped-flow kinetics measurements.

2. EXPERIMENTAL SECTION

2.1. Materials. The following synthetic procedures are adapted from Dance et al.[29,41,42] and performed in a N_2-filled glovebox (VAC atmospheres) except where noted. Thiophenol (PhSH, 99%, Acros), 4-methyl-thiophenol (*p*-Me-PhSH, 98%, Acros), triethylamine (Et_3N, 99%, Fisher), zinc nitrate hexahydrate ($Zn(NO_3)_2{\cdot}6H_2O$, Fisher), cadmium nitrate tetrahydrate ($Cd(NO_3)_2{\cdot}4H_2O$, 99+%, Acros), cobalt nitrate hexahydrate ($Co(NO_3)_2{\cdot}6H_2O$, 99+%, Acros), and tetramethylammonium chloride (NMe_4Cl, 98+%, Acros) were used as received. In our studies, we denote the tetrameric cluster $(Me_4N)_2[M_4(SPh)_{10}]$ where M = Zn^{2+}, Cd^{2+} or Co^{2+} as M-4 and diluted tetrameric clusters $(Me_4N)_2[(M_{1-x}Co_x)_4(SPh)_{10}]$ as $(M_{1-x}Co_x)$-4 cluster. ***Caution!*** *Thiophenol is extremely toxic and should be handled in accordance with the materials safety datasheet.*

Synthesis of Zn-4. PhSH (3.7 mL, 36.4 mmol) and Et_3N (5.1 mL, 36.4 mmol) were dissolved in methanol (8 mL). A solution of $Zn(NO_3)_2{\cdot}6H_2O$ (4.2 g, 14.1 mmol) in methanol (14 mL) was added to the above solution, stirred for 20 min, and followed by addition of a solution of NMe_4Cl (1.746 g, 16 mmol) in methanol (8 mL). The resulting clear solution was kept at ∼0 °C for 48 h, and white crystals formed. The crystals were removed from the glovebox to a chemical fume hood where they were filtered, washed with cold methanol to separate the unreacted precursors, and vacuum-dried. Products were left to recrystallize from a supersaturated solution in anhydrous CH_3CN with a few drops of toluene by vapor diffusion method in a freezer at ∼0 °C.

Synthesis of $(Zn_{1-x}Co_x)$-4. The procedure is the same as for Zn-4, except varying amounts of $Co(NO_3)_2{\cdot}6H_2O$ was added to the preformed Zn-4 clusters before addition of the methanolic NMe_4Cl solution. The solution immediately turned green upon addition of cobalt nitrate. We have prepared $(Zn_{1-x}Co_x)$-4 clusters where x_{nom} = 0.005, 0.01, 0.05, 0.10, 0.15, 0.20, 0.25, and 0.50. Clusters with x_{nom} > 0.01 were not recrystallized due to the sensitivity of clusters to oxidation. In all clusters with Co^{2+}, the x_{nom} value refers to the nominal cation mole fraction of $Co(NO_3)_2{\cdot}6H_2O$ added to the preformed clusters.

Synthesis of $[Zn_4(SPh)_8Cl_2](NMe_4)_2$ and $[(Zn_{1-x}Co_x)_4(SPh)_8Cl_2]$-$(NMe_4)_2$ Clusters. To a solution of PhSH (1 mL, 10 mmol), Et_3N (1.38 mL, 10 mmol), and NMe_4Cl (0.5 g, 0.45 mmol) in methanol (10 mL), $Zn(NO_3)_2{\cdot}6H_2O$ (1.5 g, 5 mmol) dissolved in methanol (15 mL) was added slowly. A white precipitate immediately formed and was dissolved by addition of acetone (10 mL). For Co^{2+} doping, $Co(NO_3)_2{\cdot}6H_2O$ dissolved in methanol was added to the preformed clusters. The solution was left at room temperature for 5 days. Crystals were washed with methanol and vacuum-dried.

Synthesis of Cd-4 and $(Cd_{1-x}Co_x)$-4. The synthetic procedure was similar to that for the Zn-4 clusters, except $Zn(NO_3)_2{\cdot}6H_2O$ was replaced by $Cd(NO_3)_2{\cdot}4H_2O$. To a solution of PhSH (4.64 mL, 45.5 mmol) and Et_3N (6.35 mL, 45.5 mmol) in methanol (15 mL), $Cd(NO_3)_2{\cdot}4H_2O$ (5.18 g, 17 mmol) in methanol (15 mL) was added dropwise. After 20 min, NMe_4Cl (2.11 g, 19.25 mmol) in methanol (10 mL) was added to the above solution. For Co^{2+} doping, $Co(NO_3)_2{\cdot}6H_2O$ dissolved in methanol was added to the preformed Cd-4 clusters before addition of the methanolic NMe_4Cl solution. Only 0.5% (x_{nom} = 0.005) and 1% (x_{nom} = 0.01) doped clusters were recrystallized.

The clusters with 4-methylbenzenethiolate (*p*-Me-PhS^-) instead of benzenethiolate (PhS^-) were synthesized using similar procedures.

Synthesis of $[Co(SPh)_4](NMe_4)_2$, Co-1. To a solution of PhSH (1.65 mL, 16 mmol), Et_3N (2.23 mL, 16 mmol), and NMe_4Cl (1.1 g, 10 mmol) in methanol (35 mL), $Co(NO_3)_2{\cdot}6H_2O$ (0.5 g, 1.7 mmol) in methanol (5 mL) was added dropwise. After 20 min, 1-propanol (25 mL) was added and the solution was left undisturbed at 0 °C for 48 h; greenish-blue crystals formed. The crystals were separated and vacuum-dried.

DOI: 10.1021/acs.inorgchem.5b00421
Inorg. Chem. 2015, 54, 5757−5767

Synthesis of Co-4. To a solution of PhSH (0.51 mL, 5 mmol) and Et_3N (0.7 mL, 5 mmol) in acetonitrile (12 mL), $Co(NO_3)_2{\cdot}6H_2O$ (0.485 g, 2 mmol) in ethanol (13 mL) at ~40 °C was added. After 20 min, a solution of NMe_4Cl (0.655 g, 6 mmol) in methanol (5 mL) at ~70 °C was added. Dark green crystals were obtained after the product solution was stored for 5 days at ~0 °C.

2.2. Physical Methods and Measurements. Absorption (Cary 50 or Varian 670 FTIR) and emission (Cary Eclipse) spectra were collected on acetonitrile solutions purged with N_2 gas. High-resolution electrospray mass spectrometry (ESI-MS) was collected in negative-ion mode with a cone voltage of 80 V and flow rate of 3 μL/min (Bruker FT-MS solariX-7T). Variable-temperature 400 MHz ^{1}H NMR studies were performed with d_3-CH_3CN (10 ± 0.02 mg sample dissolved in 0.4 mL solutions) (Bruker Avance). Stopped-flow kinetics measurements were performed using an OLIS RSM-1000 spectrophotometer in CH_3CN or dimethylformamide (DMF) solutions. Molar concentrations of cobalt in the clusters were determined quantitatively by inductively coupled plasma optical emission spectroscopy (ICP-OES, PerkinElmer Optima DV4300). The clusters were digested in 5% HNO_3 solution for ICP-OES measurements, and the measured values agree well with the nominal cation mole fractions (i.e., $x \approx x_{nom}$, see Supporting Information).

3. RESULTS AND DISCUSSION

3.1. Electronic Structures and Dopant Stability. The room temperature electronic absorption spectra of Zn-4 and Cd-4 clusters after addition of Co^{2+} ions (x_{nom} = 0.25), Co-4 clusters, and Co-1 clusters in CH_3CN are presented in Figure 1.

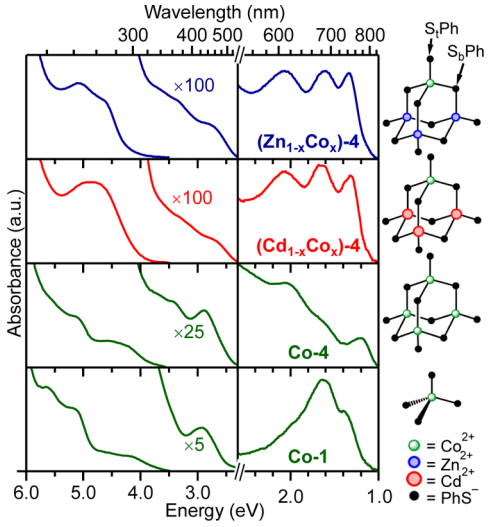

Figure 1. Electronic absorption spectra of $(Zn_{1-x}Co_x)$-4, $(Cd_{1-x}Co_x)$-4, Co-4, and Co-1 in acetonitrile at room temperature (x_{nom} = 0.25 for the two doped clusters). The spectra are separated into three regions: >3.8 eV are intense host-based LMCT transitions; between 2.5 and ~3.8 eV are weaker Co^{2+}-related transitions; <2.3 eV are ligand-field transitions associated with Co^{2+}. The optical densities in visible region are scaled by 1−2 orders of magnitude to be on the same scale as the UV transitions. Note the change in energy scaling changes at 2.3 eV denoted by the vertical line and "//" on the axes. Far right: schematic representions of the cluster and coordination environment of the Co^{2+} ions (phenyl groups omitted).

The Zn-4 and Cd-4 clusters containing Co^{2+} possess two intense transitions in the UV region greater than 4 eV that are similar to the respective spectra of the pure Zn-4 and Cd-4 clusters as shown in Figure 2. The UV transitions have been assigned previously for Zn-4 and Cd-4 to a combination of the $\pi \rightarrow \pi^*$ transition of the PhS^- and ligand-to-metal charge

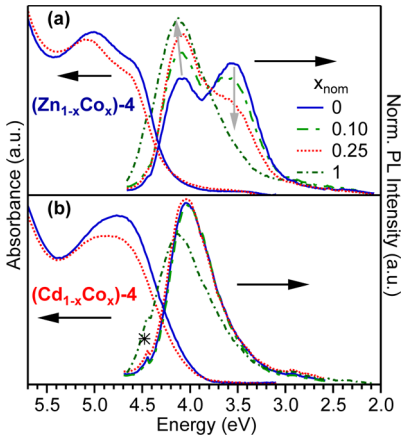

Figure 2. Room temperature electronic absorption and emission spectra ($h\nu_{exc}$ = 5.2 eV) of (a) $(Zn_{1-x}Co_x)$-4 and (b) $(Cd_{1-x}Co_x)$-4 clusters. The absorption spectra were collected at x_{nom} = 0 (—) and 0.25 (···). The emission spectra are shown with x_{nom} = 0 (—), 0.10 (– – –), 0.25 (···), and 1 (– · –). The asterisk at ~4.5 eV in the emission spectra is an artifact from a long-pass filter.

transfer (LMCT) transition.[43,44] The Co-4 and Co-1 clusters also display broad electronic transitions in the UV, but with different relative intensities compared to the Zn-4 and Cd-4 clusters and an additional transition at slightly lower energies at ~4.2 eV. These UV transitions of Co-1 and Co-4 have not been reported previously, but are similar to the other M-1 (see Supporting Information, Figure S1) and M-4 clusters, respectively.[43−46] The weaker UV transition at ~4.2 eV in the Co-1 and Co-4 clusters is of the same order of magnitude as the UV transitions and is assigned to a LMCT transition involving the empty 4s orbitals of the Co^{2+} ion. A schematic molecular orbital diagram with possible electronic transitions for the $(M_{1-x}Co_x)$-4 clusters is given in the Supporting Information (Figure S2).

The spectral region from 1.5 to 4.0 eV shows additional electronic transitions in the clusters containing Co^{2+} ions that are at least 2 orders of magnitude weaker than the UV transitions. The bands between ~2.6 and 3.8 eV are assigned as LMCT transitions from ligand-based π-orbitals of the PhS_b^- and PhS_t^- to the partially filled t_2 orbitals of the Co^{2+} ion based on previous assignment of the spectra of Co-1 and Co-4 clusters.[41,47] The structured band centered at ~1.8 eV shown on an expanded energy axis in Figure 1 is the $^4A_2(F) \rightarrow {}^4T_1(P)$ ligand field transition of the pseudotetrahedral Co^{2+} ion.[41] The energy and fine structure of the $^4T_1(P)$ transition is similar for both $(Zn_{1-x}Co_x)$-4 and $(Cd_{1-x}Co_x)$-4 clusters, but not with respect to either the pure Co-4 or Co-1 clusters.[41]

The energies of the $^4A_2(F) \rightarrow {}^4T_1(F)$ (ν_2) and $^4A_2(F) \rightarrow {}^4T_1(P)$ (ν_3) transitions occur at similar energies for both the $(Zn_{1-x}Co_x)$-4 and $(Cd_{1-x}Co_x)$-4 clusters with $\nu_2 \approx 0.93$ eV (shown in Supporting Information, Figure S3) and $\nu_3 \approx 1.80$ eV. The ligand field parameters were estimated using expressions derived by Lane and co-workers[48] in eqs 1 and 2.

$$(10Dq)^2 - 0.529(\nu_2 + \nu_3)(10Dq) + 0.294\nu_2\nu_3 = 0 \quad (1)$$

$$B = (\nu_2 + \nu_3 - 30Dq)/15 \quad (2)$$

Previously reported ligand field parameters for Co^{2+} in the Co-4 clusters are Dq = −58.8 meV and B = 68.1 meV ($|Dq|/B$ = 0.86), and in the Co-1 cluster are Dq = −50.0 meV and B = 79.7 meV ($|Dq|/B$ = 0.63).[32,47,48] Using eqs 1 and 2, we

DOI: 10.1021/acs.inorgchem.5b00421
Inorg. Chem. 2015, 54, 5757−5767

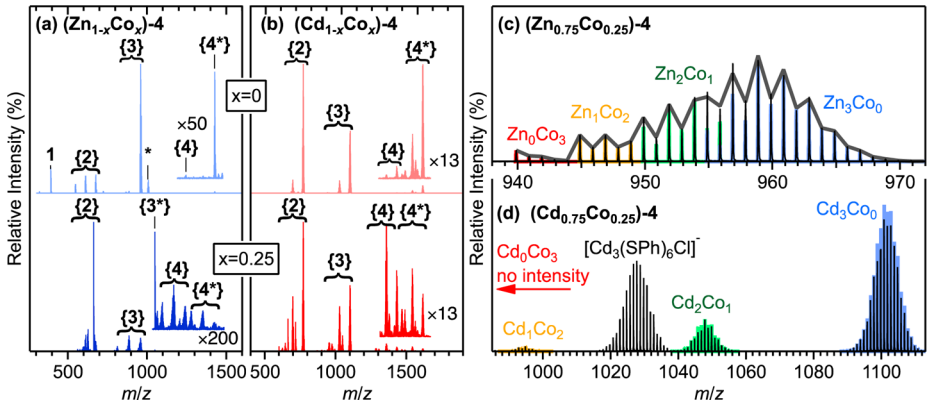

Figure 3. Negative-ion mode high-resolution ESI mass spectra of (a) $(Zn_{1-x}Co_x)$-4 and (b) $(Cd_{1-x}Co_x)$-4 for x_{nom} = 0 (top) and 0.25 (bottom). Numbers denote the value of n for the fragment with the general formula $[M_n(SPh)_{2n+1}]^-$. Additional peaks assigned to single and double Cl^- substitution for PhS^- ligands are also observed at −74 and −147 m/z from the unsubstituted cluster. For a full assignment of the spectra see Table S1 in Supporting Information. Fragments denoted with an asterisk have an extra $(NMe_4)^+$ and $(SPh)^-$. Fragmentation of $(Zn_{1-x}Co_x)$-4 and $(Cd_{1-x}Co_x)$-4 (x_{nom} = 0.25) in the m/z region of the respective $[M_3(SPh)_7]^-$ fragments are shown in (c) and (d), respectively. Simulated spectra for the fragments are shown in color behind the experimental spectra. In (c), the sum of the weighted overlapping isotopic distributions is given as a solid thick line that almost tracks the experimental peak maxima. No intensity was observed in the region of $[Co_3(SPh)_7]^-$ in (d) and is not shown.

estimate the ligand field parameters for Co^{2+} diluted in the Zn-4 and Cd-4 clusters to be Dq = −56 meV and B = 71 meV ($|Dq|/B$ = 0.79). The ligand field parameters for Co^{2+} in Zn-4 and Cd-4 are closer to Co-4 than Co-1. We also observe a gradual shift in the energy of the visible LMCT transition at ~2.7 eV toward the analogous LMCT transition in Co-4 (~2.9 eV) with increasing nominal Co^{2+} content (see Supporting Information, Figure S4). These results indicate that Co^{2+} is incorporated into the M-4 clusters.

Figure 2 shows the room temperature absorption and normalized emission spectra of $(Zn_{1-x}Co_x)$-4 and $(Cd_{1-x}Co_x)$-4 clusters in degassed CH_3CN solutions as a function of x_{nom}. Upon addition of Co^{2+} to the Zn-4 cluster we observe drastic changes to the emission spectra, but negligible changes to the absorption spectra of the UV bands. The lower energy feature of Zn-4 gradually disappears and the higher energy feature at 4.12 eV gradually shifts to the 4.14 eV emission of Co-4 with increasing x_{nom}. The normalized spectra shown in Figure 2a reveals a clear isosbestic point at ~3.8 eV that suggests the change in the emission spectra of the Zn-4 clusters is caused by Co^{2+} incorporation. The emission spectra of pure Cd-4 cluster shows a single, broad peak at ~4.03 eV that has little to no change with increasing Co^{2+} addition compared to $(Zn_{1-x}Co_x)$-4. This result suggests that the higher energy 4s orbitals of Zn compared to the 5s orbitals of Cd have a significant effect on the relative emission intensities.

Türk and co-workers reported weak emission centered at 3.4 eV for the Zn-4 cluster and ~2.5 eV for the Cd-4 clusters from *aerated* acetonitrile solutions under 4.0 eV excitation.[43,45] The 2.5 eV emission peak of Cd-4 shifts to 3.5 eV (with a shoulder at 2.8 eV) upon exposure to UV irradiation and was attributed to the formation of thianthrene, benzothiophene, and benzenethiol photoproducts. We did not observe the formation of these photoproducts under anaerobic excitation. Here, we observe two peaks in the UV region for Zn-4 in contrast to the previous reports and assign the emission bands to the radiative recombination from the LMCT and intraligand excited states. We are currently investigating the nature of these transitions in the Co^{2+}-doped clusters using time-resolved and temperature-dependent steady-state spectroscopies and time-dependent density functional theory calculations that will be published elsewhere.

The stability of the Co-1, Co-4, and $(M_{1-x}Co_x)$-4 clusters was determined by monitoring the Co^{2+} ligand field absorption kinetics in aerated CH_3CN solutions over time. The absorption spectra of $(Zn_{1-x}Co_x)$-4 and $(Cd_{1-x}Co_x)$-4 (x_{nom} = 0.01) clusters show no change in the ligand field or low-energy charge transfer transitions over the course of 5 days. However, the spectra of the neat Co-1 and Co-4 clusters slowly convert from tetrahedral coordination (in the M-4 clusters) to octahedral coordination (free in solution) over the course of about 28 h (see Supporting Information, Figure S5). We also monitored the thermal stability of clusters in CH_3CN by heating the solutions up to 80 °C, and no spectral changes were observed upon cooling back to room temperature. These results confirm that the Zn-4 and Cd-4 clusters and the cobalt ions inside the clusters are stable in the presence of a coordinating solvent.

To understand the effect of temperature on the relative yield for Co^{2+} exchange into these clusters, we performed the exchange experiment at different temperatures (22, 30, 35, and 50 °C) and x_{nom} = 0.05. The relative concentration of the Co^{2+} per cluster was estimated by comparing the Co^{2+} ligand field intensities of the absorption spectra after normalizing for the cluster absorption in the UV region. The following trend in relative Co^{2+} ligand field absorption (concentration) was obtained: for $(Zn_{1-x}Co_x)$-4 the relative Co^{2+} concentration increased gradually from 3.3 (22 °C), 3.4 (30 °C), and 5.0 (50 °C), and for $(Cd_{1-x}Co_x)$-4 the trend increased much faster having values of 1 (22 °C), 3.57 (35 °C), and 5.71 (50 °C). At room temperature, more Co^{2+} is incorporated into the Zn-4 cluster than into the Cd-4 cluster, but at 50 °C the exact opposite is observed. This observation suggests a significant difference in solution behavior and equilibrium dynamics between the clusters at higher temperatures. The origin of this difference will be elaborated upon in section 3.6.

3.2. Electrospray Ionization Mass Spectrometry. The mass spectra of these clusters provide important information about the structure and thermodynamic stability of the mixed metal clusters compared to the pure, host clusters.[49] The high-resolution ESI mass spectra of $(Zn_{1-x}Co_x)$-4 and $(Cd_{1-x}Co_x)$-4 molecular clusters (x_{nom} = 0 and 0.25) in negative-ion mode at

DOI: 10.1021/acs.inorgchem.5b00421
Inorg. Chem. 2015, 54, 5757−5767

a cone voltage of 80 V are shown in Figure 3. Mass spectra collected at other Co^{2+} mole fractions ($0 \leq x_{nom} \leq 0.5$) are given in Supporting Information (Figures S6 and S7). At a cone voltage of 80 V, the molecular clusters yield numerous negatively charged fragments with the general formula $[M_n(SPh)_{2n+1}]^-$ (n = 1−4) and $(NMe_4)[M_4(SPh)_{10}]^-$. The dominant fragments of Zn-4 and $(Zn_{1-x}Co_x)$-4 (x_{nom} = 0.25) are the n = 3 (m/z 960) and n = 2 (m/z 667) fragments, respectively. For both Cd-4 and $(Cd_{1-x}Co_x)$-4 (x_{nom} = 0.25) the dominant fragment is the n = 2 fragment (m/z 771). The parent ion fragments $(NMe_4)[M_4(SPh)_{10}]^-$ are observed in all clusters at m/z 1616 (Cd-4) and m/z 1426 (Zn-4). Detailed investigations of the pure Zn-4 and Cd-4 clusters by positive and negative mode ESI-MS have been previously reported.[49,50] The results shown in Figure 3 for the pure Zn-4 and Cd-4 clusters are similar to the previously reported mass spectra. Additional fragments from single and double Cl^- ligand exchange with PhS_t^- in the diluted $(M_{1-x}Co_x)$-4 clusters are observed at −74 and −147 m/z units, respectively, from the n = 2, 3, and 4 fragments (see Figure 3 and Supporting Information, Table S1). However, noticeably absent from the larger fragments such as $[(M_{1-x}Co_x)_3(SPh)_7]^-$ is intensity in the mass spectra corresponding to the exchange of a third Cl^- ligand, that is, $[(M_{1-x}Co_x)_3(SPh)_4Cl_3]^-$. This result is consistent with Dance's observation that the maximum substitution number of Cl^- ligands into the Zn-4 cluster is two.[42]

The spectra shown in Figure 3 were analyzed to determine if fragments indicating Co^{2+} substitution into the M-4 clusters are present and their relative yield. Figure 3c,d displays the region of the mass spectra where the $[(M_{1-x}Co_x)_3(SPh)_7]^-$ fragments for M = Zn and Cd with x_{nom} = 0.25. The appearance of pure $[M_3(SPh)_7]^-$ fragments is observed in both spectra. The $[Co_3(SPh)_7]^-$ fragment is observed in the mass spectrum of the $(Zn_{1-x}Co_x)$-4 cluster, but is not in the mass spectrum of $(Cd_{1-x}Co_x)$-4 cluster. In addition to these pure cobalt species, we can clearly observe Co substitution into the n = 3 fragments of both Zn-4 and Cd-4 clusters in the regions of the $[M_2Co_1(SPh)_7]^-$ and $[M_1Co_2(SPh)_7]^-$ ions. Co^{2+}-substituted n = 2 fragments are also positively identified in the ESI-MS and are shown in Supporting Information (Figure S8).

Quantitative analysis of the compositions of the n = 2 and 3 fragments presents clear trends when plotted as a function of the nominal Co^{2+} content (x) added to the Zn-4 and Cd-4 clusters. Figure 4 shows the relative intensities of the $[(M_{1-x}Co_x)_n(SPh)_{2n+1}]^-$ fragments with unique compositions for n = 2 (x_{nom} = 0, 0.5, and 1) and n = 3 (x_{nom} = 0, 1/3, 2/3, and 1). The relative intensities of the pure host fragments (x_{nom} = 0) for both n = 2 and 3 always decrease faster for the pure Zn fragments compared to the Cd fragments with increasing x. As a result, the relative intensities of Co-substituted fragments are therefore always greater for the $(Zn_{1-x}Co_x)$-4 clusters than for the $(Cd_{1-x}Co_x)$-4 clusters, which suggests that the equilibrium constant describing Co^{2+} substitution into the Zn-4 cluster is favorable compared to the Cd-4 cluster in the low doping regime where on average only one Co^{2+} may substitute into the cluster. We have shown that ESI-MS is an informative analytical technique to determine unique dopant compositions in the clusters after the cation exchange reactions. However, it provides no information regarding the dynamics of the equilibrium; therefore, we studied the dynamics of these clusters by NMR spectroscopy.

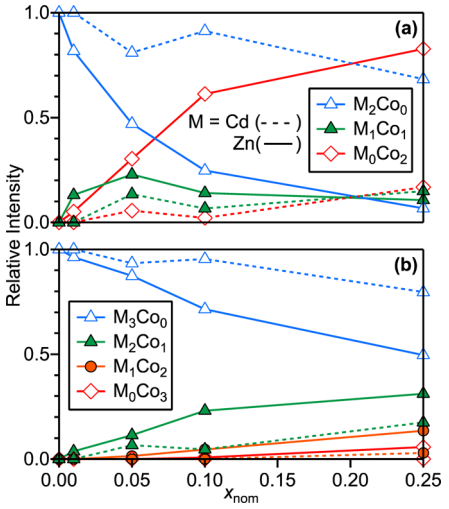

Figure 4. Relative intensity of the different possible compositions of (a) n = 2 and (b) n = 3 benzenethiolate species from single value decomposition analysis of the mass spectra of $(Zn_{1-x}Co_x)$-4 (solid lines) and $(Cd_{1-x}Co_x)$-4 (dashed lines) as a function of x_{nom}. The lines are guides to the eye. The symbols are defined in the boxes of each panel.

3.3. Nuclear Magnetic Resonance (NMR) Spectroscopy. The 400 MHz ^1H NMR spectra of pure (Zn-4, Cd-4, Co-4, and Co-1) and diluted clusters ($(Zn_{1-x}Co_x)$-4 and $(Cd_{1-x}Co_x)$-4 where x_{nom} = 0.01) are shown in Figure 5. The pure Zn-4 and Cd-4 clusters display overlapping multiplets in the region between 6 and 8 ppm for the aromatic protons on the inequivalent PhS_b^- and PhS_t^- ligands as observed previously (for a schematic structure of the cluster, see Figure 1).[30] The antiferromagnetic exchange coupling between Co^{2+} ions mediated by the PhS_b^- ligands in the Co-4 cluster results in an S = 0 ground state at cryogenic temperatures. At 245 K, however, the Co-4 clusters are weakly paramagnetic and the proton resonances of the benzenethiolate ring shift to $\delta_{Co\text{-}4}$ = 13.2 (m-H_t), 11.2 (m-H_b), −12.8 (p-H_t), −16.6 (p-H_b), −18.4 (o-H_t), and −28.4 ppm (o-H_b) in agreement with previously reported spectra.[30,51−53] The line widths ($\Delta\nu$) of the proton resonances on the PhS^- ring of Co-4 and Co-1 increase in the order p-H ≈ m-H < o-H (see Supporting Information, Table S2). The spectrum of the Co-1 monomer complex is simplified by the presence of equivalent PhS^- ligands, and peak assignments are unambiguous based on line widths and relative peak areas.

When Co^{2+} is introduced into the diamagnetic Zn-4 or Cd-4 cluster, we observe larger chemical shifts of the benzenethiolate protons compared to Co-4 or Co-1. The o- and p-H's shift upfield while the m-H's shift downfield, with the latter observation in agreement[30,51] with previous results on mixtures of M-4 (M = Cd, Zn) and Co-4. The assignments of the o- and p-H's have not been reported. Therefore, the assignment of the o- and p-H's is trivial in the spectra considering relative line widths and intensities. In contrast to the assignment of the Co-4 resonances where the largest shift is assigned to a PhS_b^- ligand, we assign the larger chemical shifts to protons located on terminal PhS^- ligands for the $[M_3Co_1(SPh)_{10}]^{2-}$ species (see Figure 5). In rationalizing this assignment we consider the reduced negative charge on the bridging benzenethiolate ligand[41] to be critically important. When a benzenethiolate ligand is bridging a Co^{2+} ion and a diamagnetic ion in the

DOI: 10.1021/acs.inorgchem.5b00421
Inorg. Chem. 2015, 54, 5757−5767

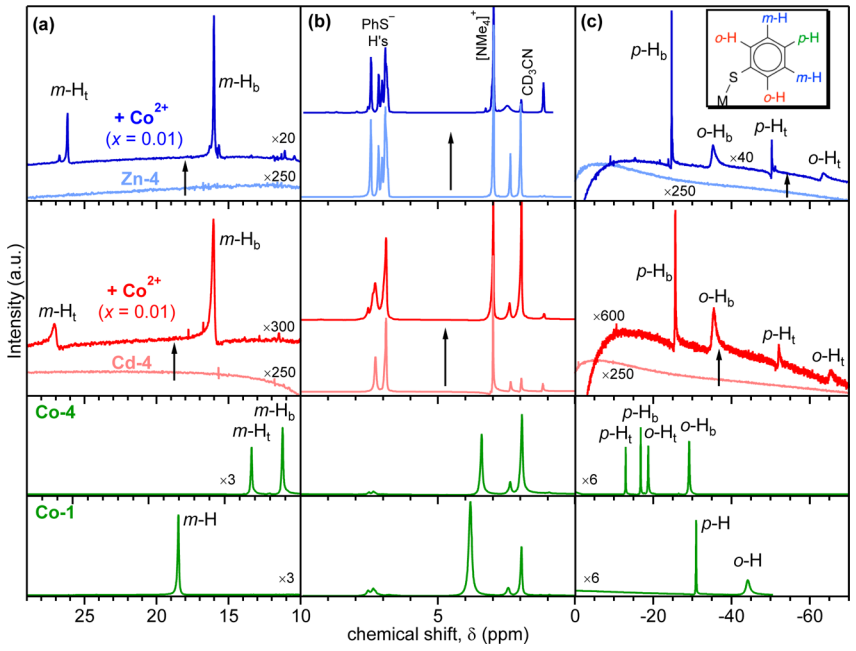

Figure 5. 400 MHz ^{1}H NMR spectra of Zn-4, $(Zn_{1-x}Co_x)$-4 (x_{nom} = 0.01), Cd-4, $(Cd_{1-x}Co_x)$-4 (x_{nom} = 0.01), Co-4, and Co-1. Sample concentrations were all 10 mg in 0.4 mL of d_3-CH_3CN. The Zn-4 and Cd-4 were collected at room temperature, while the Co-containing complexes were all collected at 245 ± 1 K. The spectra are divided into three regions from (a) δ = 27 to 10 ppm, (b) 10 to 0 ppm, and (c) 0 to −70 ppm (note that the tick spacing changes in each panel). Region b corresponds to the typical "diamagnetic" proton shifts of the benzenethiolates, Me_4N^+, and CH_3CN. Regions c and a correspond to the *o*- and *p*-, and *m*-positions of the phenyl ring, respectively, of benzenethiolate protons that are bound directly to Co^{2+} ions in the cluster. See Supporting Information (Table S2) for a summary of the peak assignments. Inset at top-right panel shows the arrangement of the benzenethiolate protons.

diluted cluster (Co^{2+}−PhS_b^-−M^{2+}), the degree of the spin density that is delocalized onto the protons of the PhS_b^- ligand will be reduced compared to Co^{2+}−PhS_b^-−Co^{2+} in Co-4. Our assignments are further supported by substitution of CH_3 at the para position of benzenethiolate which will be discussed in section 3.4. All paramagnetically shifted resonances are noticeably broader for the $(Cd_{1-x}Co_x)$-4 clusters compared to $(Zn_{1-x}Co_x)$-4 clusters for the same x_{nom} and temperature. This observation is caused by the faster PhS_b^- ↔ PhS_t^- ligand interconversion of Cd-4 compared to Zn-4.[30,54] Both $(M_{1-x}Co_x)$-4 clusters shown in Figure 5 possess no signatures of the pure Co-4 or Co-1 resonance peaks. The lack of Co-4 cluster formation is consistent with the scenario in which solvated Co^{2+} exchanges with M-4 clusters in the absence of free PhS^- until equilibrium is reached.

Figure 6a shows the ^{1}H NMR spectra at 245 ± 1 K in the regions of the *m*-H_t and *p*-H_t of $[M_3Co_1(SPh)_{10}]^{2-}$as the amount of Co^{2+} is increased in the $(M_{1-x}Co_x)$-4 cluster from x_{nom} = 0 to 0.5. The small shifts of the peak position are caused by slight temperature variations among the samples. At x_{nom} = 0.005, there is a single strong resonance observed for the *m*- and *p*-H's of the PhS_t^- ligand in both the $(Zn_{1-x}Co_x)$-4 and $(Cd_{1-x}Co_x)$-4 clusters. However, with increasing x_{nom} the number of resolved peaks increases sequentially to a maximum of four equally spaced resonances[55] (peak-to-peak separation of 222 ± 12 Hz) when $x_{nom} \geq 0.15$. This behavior is inconsistent with the expectation of simple triplets for both *m*-H and *p*-H resonances and previous reports where resolved resonances were not observed.[30] The relative intensities of the peaks also change with increasing x_{nom} (see Supporting Information, Figure S9). The transition at δ = 26 ppm has been previously assigned[30] to the *m*-H_t resonance of a PhS_t^- bound to the Co^{2+} ion of the $[Zn_3Co_1(SPh)_{10}]^{2-}$ cluster. The *m*-H_t resonance

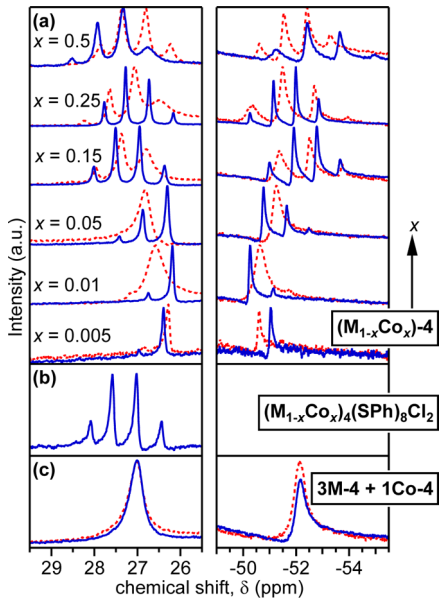

Figure 6. 400 MHz ^{1}H NMR spectra collected at 245 ± 1 K in the region of the (left panel) *m*-H_t and (right panel) *p*-H_t regions of (a) $(M_{1-x}Co_x)$-4 (M = Zn (blue, solid lines), Cd (red, dotted lines)) with varying x_{nom}, (b) recrystallized $(Me_4N)_2[(M_{1-x}Co_x)_4(SPh)_8Cl_2]$ (x_{nom} = 0.05), and (c) the product formed after mixing recrystallized M-4 and Co-4 in a molar ratio of 3:1 (same procedure as in ref 30) in d_3-CH_3CN. The small shift in low ppm transition is from differences in acquisition temperature. Note that the tick spacing of the *x*-axis is the same (0.5 ppm/tick), but the overall range in chemical shift is different for the left and right panels.

positions of $[Zn_2Co_2(SPh)_{10}]^{2-}$ and $[Zn_1Co_3(SPh)_{10}]^{2-}$ are at δ = 15.9 ppm and δ = 14.5 ppm, respectively,[30] which is well

DOI: 10.1021/acs.inorgchem.5b00421
Inorg. Chem. 2015, 54, 5757−5767

outside the range of resonances shown in Figure 6a. Therefore, the origin of these multiple resonances has to arise from protons on the terminal benzenethiolate ligand bound to Co^{2+} in $[M_3Co_1(SPh)_{10}]^{2-}$. To rule out possible intermolecular effects, we measured the NMR spectra of the $(Zn_{1-x}Co_x)$-4 clusters with x_{nom} = 0.15 after a 10-fold dilution. We observed no change in either the number of resonances or their relative areas. As a control we prepared the dichloro-substituted clusters and the ^{1}H NMR spectra of $(NMe_4)_2[(M_{1-x}Co_x)_4(SPh)_8Cl_2]$ (x_{nom} = 0.05) display the identical quartet (peak-to-peak separation of 221 ± 15 Hz) in the region of the *m*-H_ts (see Figure 6b). Reproducing previous cation exchange experiments[30] by mixing recrystallized M-4 and Co-4 clusters in a 3:1 ratio did not produce the quartet resonance for the *m*-H_t as shown in Figure 6c. Therefore, we can assign both the increase in the number of peaks and their relative areas with increasing x_{nom} to structural variation and ligand substituted $[M_3Co_1(SPh)_8Cl_2]^{2-}$ clusters. We know from the ESI-MS results above that Cl^- ligand exchange occurs after addition of NMe_4Cl to precipitate the clusters from methanol.

To gain additional insight regarding the solution dynamics of these clusters, we performed variable-temperature ^{1}H NMR measurements (VT-NMR) on $(Zn_{1-x}Co_x)$-4 and $(Cd_{1-x}Co_x)$-4 clusters (x_{nom} = 0.01 and 0.05) between 240 and 317 K in d_3-CH_3CN (spectra shown in Supporting Information, Figure S10). The Curie plot shown in Figure 7 shows that all of the

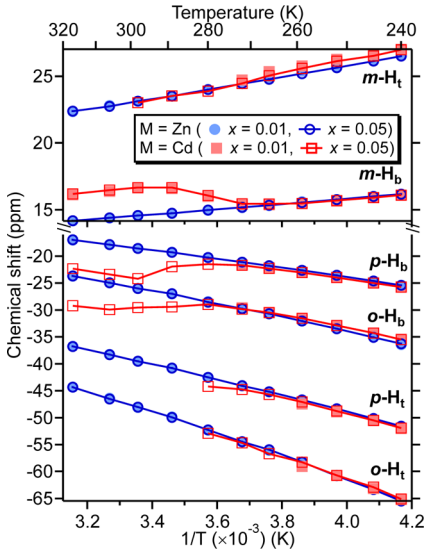

Figure 7. Temperature dependence of the chemical shifts for the PhS_b^- and PhS_t^- protons of $(Zn_{1-x}Co_x)$-4 (blue circles) and $(Cd_{1-x}Co_x)$-4 (red squares) with x_{nom} = 0.01 (filled) and 0.05 (unfilled with line). The lines are guides to the eye only. The relative scales for the *m*-H's is expanded by a factor of ~3 compared to the *o*-H's and *p*-H.

chemical shifts follow the expected Curie behavior ($\Delta\nu \propto T^{-1}$) when M = Zn, but not when M = Cd. For the $[Cd_3Co_1(SPh)_{10}]^{2-}$ cluster, the initial behavior is Curie-like, but at ~270 K, the protons on the PhS_b^- ligands shift toward the PhS_t^- positions. Concomitant with this shift is a broadening of the resonances and decrease in intensity of the PhS_t^- protons with eventual disappearance. The Curie behavior of the remaining broad resonance continues above 300 K. This temperature dependence is a clear indication of coalescence of the PhS_t^- and PhS_b^- ligands of the $[Cd_3Co_1(SPh)_{10}]^{2-}$ cluster. The position of the resonance at coalescence for the benzenethiolate ligands is weighted more to the bridging ligands because of the 3:1 ratio of bridging to terminal ligands bound to the Co^{2+} ion in the cluster (see Figure 5 and Supporting Information, Table S2). To rule out possible cluster degradation during the experiment, we collected the spectra upon cooling the sample after heating to 317 K. The temperature dependence of the NMR spectra of the $[Cd_3Co_1(SPh)_{10}]^{2-}$ cluster is quantitatively reversible. No such coalescence was detected in any of the $(Zn_{1-x}Co_x)$-4 clusters (x_{nom} = 0, 0.25, or 1).

Hagen and co-workers observed only broad resonances in the region of the benzenethiolate protons in the NMR spectrum of Cd-4 down to 239 K, indicating that the PhS_b^- and PhS_t^- ligands are undergoing fast interconversion.[30] In contrast, resolved sets of resonances for the inequivalent PhS_b^- and PhS_t^- ligands of the Zn-4 cluster were observed up to 322 K, where the peaks coalesce to give broad resonances. Behavior similar to Zn-4 was observed for the Co-4 cluster, but with no detectable coalescence up to 340 K. Coalescence of the benzenethiolate resonances is only observed for the ligands bound to Co^{2+} in the $[Cd_3Co_1(SPh)_{10}]^{2-}$ cluster at ~280 K. No coalescence is detected for the $[Zn_3Co_1(SPh)_{10}]^{2-}$ cluster up to 317 K. VT-NMR measurements of the equilibrium compositions after mixing M-4 and Co-4 clusters in a 3:1 ratio also show similar deviation from Curie behavior. The $PhS_b^- \leftrightarrow PhS_t^-$ coalescence temperature is again ~277 K for 3Cd-4:1Co-4 and >317 K for the 3Zn-4:1Co-4 mixed tetrameric clusters (data not shown). The intramolecular rearrangement rates increase with increasing size of the metal ion.[56] The intramolecular rearrangement of the (Cd_3Co_1)-4 cluster decreases significantly due to the exchange of Co^{2+} (r = 0.72 Å) in the place of the larger Cd^{2+} ion (r = 0.92 Å).[57] This result provides further spectroscopic evidence to support our argument that the electronic structure and solution dynamics of the Cd-4 cluster are significantly perturbed upon cation exchange with Co^{2+}.

3.4. Effect of Para-Substituted Benzenethiolates on Cluster Solution Dynamics. We investigated the effect of para substituent of the PhS^- ligand on the cluster electronic structures and cation exchange dynamics in solution. The introduction of electron-donating or -accepting substituents on the PhS^- ligand changes the charge on sulfur atom and energy of the highest occupied molecular orbital (HOMO)−lowest unoccupied molecular orbital (LUMO) levels. The crystallization process restricted our analysis to only *p*-Me-PhS^- cluster, which has a Hammett constant[58] of σ = −0.17. A slight decrease in the energy of visible LMCT transition for the *p*-Me substituted cluster was observed (see Supporting Information, Figure S11a), which we attribute to the increase of the HOMO level (−8.191 eV) compared to the unsubstituted benzenethiolate (−8.436 eV). We estimated the relative Co^{2+} incorporation into the *p*-Me substituted clusters, $(M_{1-x}Co_x)$-4-Me, as a function of x_{nom} using the ligand field spectral analysis as done above for the $(M_{1-x}Co_x)$-4 clusters (see section 3.1, temperature dependence at 22 °C). The $(M_{1-x}Co_x)$-4-Me clusters have 2.2 times more internal Co^{2+} than the $(M_{1-x}Co_x)$-4 clusters when M = Zn and 7 times when M = Cd. These results indicate that Co^{2+} exchange is more favorable with the Cd-4-Me clusters than with Zn-4-Me, which is opposite to the behavior of the unsubstituted clusters. A more likely explanation is that, for the $(Cd_{1-x}Co_x)$-4-Me clusters, the electron-donating *p*-Me substituent changes the

DOI: 10.1021/acs.inorgchem.5b00421
Inorg. Chem. 2015, 54, 5757−5767

softness of sulfur atom and M−SPh bond strengths that ultimately affect the efficiency of the cation exchange reaction.

Figure S11b,c in the Supporting Information presents ^{1}H NMR spectra of $(M_{1-x}Co_x)$-4-Me compared to $(M_{1-x}Co_x)$-4 clusters with x_{nom} = 0.05. The *p*-H's at −25 and −50 ppm in the $(M_{1-x}Co_x)$-4 spectra disappear in the *p*-Me substituted clusters, and the *p*-Me protons appear downfield at +30 and ∼+52 ppm for the bridging and terminal benzenethiolates, respectively. The resonances also support our assignments for the *o*- and *p*-H's in the $(M_{1-x}Co_x)$-4 clusters shown in Figure 5. The coalescence temperature from the VT-NMR measurements was found to be ∼289 K for the (Cd_3Co_1)-4-Me clusters, and no coalescence was observed until 317 K in (Zn_3Co_1)-4 clusters. The slight increase in the coalescence temperature suggests that the ligand interconversion rate is slower when electron-donating groups are substituted on the phenyl ring that is likely caused by stronger Cd−SR bond in the (Cd_3Co_1)-4-Me cluster. Our observations indicate that the electronic properties of the benzenethiolate ligands can have a significant effect on the solution dynamics of the clusters, although more ligand systems need to be studied to strengthen this conclusion.

3.5. Reversibility of the Cation Exchange Reaction. The balanced equilibrium expression describing the cation exchange is given by (3):

$$\text{M-4} + x\text{Co}^{2+} \rightleftharpoons (M_{1-x}Co_x)\text{-4} + x\text{M}^{2+} \quad (3)$$

To test whether the equilibrium of these molecular clusters can be biased to favor reactants, we studied the reverse exchange reaction, which removes Co^{2+} from the cluster by simply adding excess amounts of M^{2+}. Figure 8a,b shows the electronic absorption spectra of pure metal clusters, after exchange with Co^{2+} (x_{nom} = 0.05), and after reversible exchange with an excess of M^{2+}. The electronic transitions in the UV region (intraligand and CT transitions) from the host cluster are nearly unchanged throughout both exchange reactions, which indicates that the structure of the host is likely preserved during the cation exchange and reversible exchange processes. The Co^{2+} ligand field transitions in the spectra clearly indicate Co^{2+} substitution after the cation exchange reaction, but they disappear completely after the M^{2+} reversible exchange reaction. The speciation of paramagnetic dopants in these clusters was also monitored by ^{1}H NMR as shown in Figure 8c,d. The exchange of Co^{2+} for M^{2+} in the M-4 clusters results in strong paramagnetic chemical shifts as discussed above. After the reversible exchange of M^{2+} for Co^{2+}, the shifted signals disappear. The optical absorption spectra and ^{1}H NMR spectra confirm that the reaction product is M-4 after the reversible exchange and the cluster morphology is preserved during the exchange process.

To determine the relative amounts of Zn^{2+} and Cd^{2+} required to displace the Co^{2+} in the respective M-4 cluster, we performed a titration experiment. These experiments were done by adding incremental amounts of $M(NO_3)_2$ salts dissolved in either DMF or CH_3CN to the $(M_{1-x}Co_x)$-4 clusters with x_{nom} = 0.05 and following the reaction by electronic absorption spectroscopy. The Co^{2+} $^4A_2 \rightarrow {}^4T_1(P)$ ligand field absorption band assigned to the Co^{2+} in the cluster at 1.8 eV decreases in intensity with increasing M^{2+} addition for both $(M_{1-x}Co_x)$-4 clusters. As the amount of tetrahedral Co^{2+} decreases to zero, a weak absorption band at ∼2.3 eV grows in intensity that is consistent with octahedral Co^{2+} (spectra shown in Supporting Information, Figure S12). Figure 9 plots the normalized absorption of the Co^{2+} $^4A_2 \rightarrow {}^4T_1(P)$ transition as a function of the equivalents of M^{2+} added to the $(M_{1-x}Co_x)$-4 clusters. The amount of M^{2+} needed to remove the Co^{2+} from the clusters is very different and depends on the identity of the M^{2+} ion. The amount of added Cd^{2+} was ∼30 times more than the initial amount of Co^{2+} in the cluster. For Zn^{2+}, this ratio is significantly higher at ∼250 equiv of Co^{2+} needed to obtain the pure M-4 cluster. We performed this experiment also with the 4-methyl-benzenethiolate analogues and observed similar

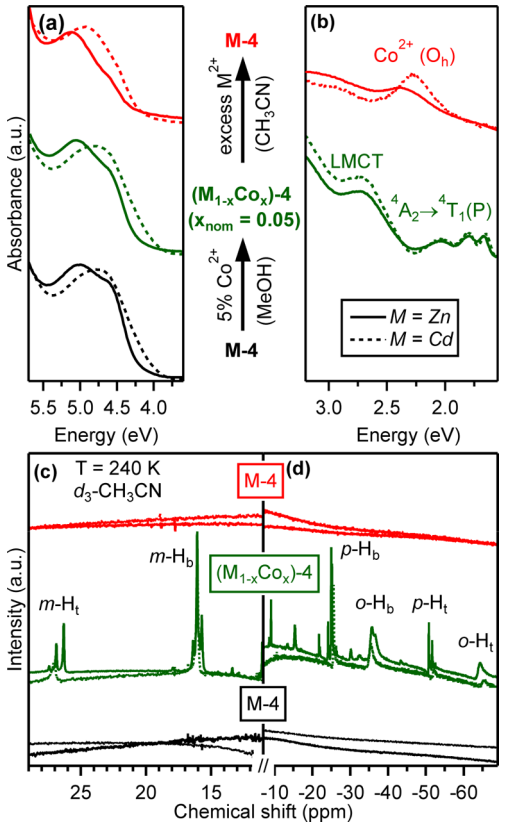

Figure 8. (a, b) Room-temperature electronic absorption spectra and (c, d) 400 MHz ^{1}H NMR spectra at 240 K in d_3-CH_3CN of the M-4 clusters before (bottom spectra in each panel) and after addition of x_{nom} = 0.05 Co^{2+} (middle), and after addition of a large excess host M^{2+} cation (top). The solid lines denote the spectra for the Zn-4 clusters, and the dashed lines denote the Cd-4 clusters.

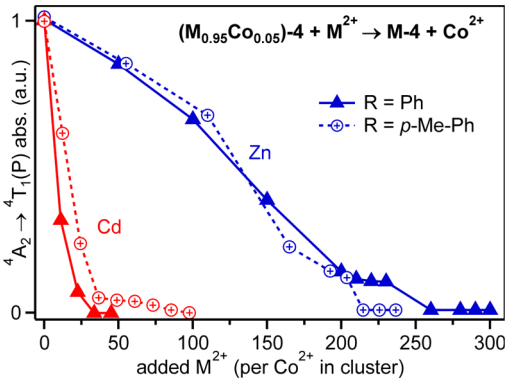

Figure 9. Relative optical densities for the Co^{2+} ligand field transitions in the clusters as a function of M^{2+} added to $[(Zn_{1-x}Co_x)_4(SR)_{10}]$ (blue) and $[(Cd_{1-x}Co_x)_4(SR)_{10}]$ (red) where R = Ph (triangles with solid lines) and *p*-Me-Ph (circles with dashed lines).

DOI: 10.1021/acs.inorgchem.5b00421
Inorg. Chem. 2015, 54, 5757−5767

behavior for the disappearance of the tetrahedral Co^{2+} in both clusters with added M^{2+}.

The cation exchange rates are much faster in colloidal nanocrystals (<1 s) compared to bulk semiconductors (several hours to weeks) at room temperature due to the large surface-to-volume ratio of nanocrystals.[24−26] To determine the rates of the cation exchange reactions in these molecular clusters, we measured the kinetics of the appearance of the Co^{2+} ligand field transition at 1.8 eV (λ = 690 nm) by stopped-flow measurements in CH_3CN (see Supporting Information, Figure S13). The cation exchange reaction for Cd-4 with Co^{2+} is faster than the instrument response time placing a lower limit on the rate of $k_{obs} > 10^3\ s^{-1}$. The cation exchange reaction for the Zn-4 clusters with Co^{2+} shows single-exponential growth of the ligand field transition with time and a rate constant of $k_{obs} = 7.7\ s^{-1}$. The observed rate constant increases for the Co^{2+} exchange reaction with the *p*-Me substituted Zn-4 clusters ($k_{obs} = 9.9\ s^{-1}$) and dichloro ligand substituted Zn-4 clusters ($k_{obs} = 11.6\ s^{-1}$). These data suggest that the identity of the benzenethiolate ligands may be a viable way to manipulate the reactivity of the tetrameric clusters.

3.6. Mechanism of Co^{2+} Incorporation into the Zn-4 and Cd-4 Molecular Clusters. Two possible mechanisms for cation exchange of Co^{2+} into $(Me_4N)_2[Zn_4(SPh)_{10}]$ clusters have been proposed by Autissier and Henderson.[51] The first mechanism is associative and involves the attack of M^{2+} at the sulfur of a bridging benzenethiolate. The second mechanism involves the initial cleavage of a bridging thiolate followed by Co^{2+} association forming a $[M_4(SPh)_{10}]\cdot Co^{2+}$ intermediate species. The reaction rates of the elementary steps are different in these two mechanisms in terms of either bond-making of benzenethiolates to the incoming Co^{2+} or bond-breaking of $M-S_bPh$ bond in the M-4 host cluster. Our results provide insight into the kinetics and thermodynamic stabilities between Zn-4 and Cd-4 clusters. Specifically, we observed a strong temperature dependence of the $PhS_t^- \leftrightarrow PhS_b^-$ ligand interconversion rate with the identity of the M^{2+} ion (rates of interconversion, Cd-4 ≫ Zn-4 > Co-4). The mechanism of the $PhS_t^- \leftrightarrow PhS_b^-$ interconversion has been proposed previously and involves the concerted breaking of two $M-PhS_b^-$ bonds followed by 120° rotation about the remaining $M-S_bPh$ bond.[30] The faster interconversion rate for Cd-4 results in faster exchange kinetics than the stopped-flow instrument limits ($k_{obs} > 10^3\ s^{-1}$). The ligand-field analysis and ESI-MS results suggest, however, that the exchange is inefficient and results in low yields for Co^{2+} incorporation into Cd-4. Therefore, the equilibrium reaction defined by eq 3 above is fast in the forward direction when M = Cd, but the equilibrium constant is relatively low.

We estimate the rate of cation exchange is at least 2 orders of magnitude slower when M = Zn ($k_{obs} = 7.7\ s^{-1}$ for PhS^-) that we attribute to the slower ligand interconversion rate as determined from NMR spectroscopy.[59] While the cation exchange reaction is slow for the Zn-4 cluster, the ESI-MS indicates that the equilibrium favors $(Zn_{1-x}Co_x)$-4 compared to $(Cd_{1-x}Co_x)$-4 as the result of reduced strain in the molecular structure when the host and dopant have similar covalent radii. These observations provide strong evidence that the solution chemistry of these molecular clusters is largely dependent on the identity of the host metal ion. In other words, when M = Zn the equilibrium with Co^{2+} is static and when M = Cd the equilibrium with Co^{2+} is dynamic.

Using the above arguments, we can predict the behavior of the $(M_{1-x}Co_x)$-4 clusters. Based on VT-NMR studies, the coalescence temperature of the $PhS_t^- \leftrightarrow PhS_b^-$ ligands in the M = Zn clusters was not observed up to 317 K, but was observed at ∼280 K for the $(Cd_{1-x}Co_x)$-4 species. We were unable to detect rates for the reverse exchange reactions, so instead we performed a titration study to determine the critical relative equivalents of M^{2+} needed to remove all Co^{2+} from the $(M_{1-x}Co_x)$-4 clusters. The results presented in Figure 9 are consistent with our position that the equilibrium is more static when M = Zn compared to Cd.

Reversible exchange of M^{2+} with Co^{2+} in the molecular clusters can also be explained by the associative and dissociative mechanisms described above,[51] but the kinetics and thermodynamics can also be explained by hard−soft acid−base (HSAB) principles. Within the basis of HSAB theory, Co^{2+} and Zn^{2+} are both borderline acids and Cd^{2+} is a soft acid (SA). Thus, in the reverse exchange reaction, equilibrium is favored toward Zn-4 only after a large excess amount of Zn^{2+} in CH_3CN (HB) was added to overcome the similar acid−base interactions between Co^{2+} and PhS^- (SB). Likewise, the reverse exchange reaction of $(Cd_{1-x}Co_x)$-4 needed less Cd^{2+} because of the stronger attraction between Cd^{2+} (SA) and PhS^- (SB) compared to Cd^{2+} with DMF (HB). In general, excess amount of metal is necessary to lower the chemical formation energy for removing dopant ions inside the molecular cluster. Here we demonstrated the cation exchange and reverse cation exchange reactions at the molecular scale are not limited by the size of the metal. Changing the terminal ligands from PhS^- to *p*-Me-PhS^- or Cl^- plays less of a role in determining cation exchange rates based on the limited examples we have studied here. Controlling the charge density (softness or hardness) of the chalcogenolate ligands with appropriate substituents may lead to novel single-source precursors for preparing DMS-QDs with homogeneous dopant distributions up to the solid solubility limit.

4. CONCLUSIONS

Here, we presented the successful demonstration of cation exchange reactions in Zn-4 and Cd-4 benzenethiolate molecular clusters. Ligand-field absorption spectroscopy of $(M_{1-x}Co_x)$-4 clusters is consistent with the Co^{2+} in a pseudotetrahedral site. Despite many similarities in the ligand field and low energy LMCT transitions, we presented many instances where subtle or significant differences in the electronic structures between $(Zn_{1-x}Co_x)$-4 and $(Cd_{1-x}Co_x)$-4 are apparent. Differences in the luminescence spectra are one such example where the $(Zn_{1-x}Co_x)$-4 clusters gradually change from having two emissive states when $x_{nom} < 0.25$ to only one emissive state at $x_{nom} = 1$. In contrast, the $(Cd_{1-x}Co_x)$-4 clusters show a negligible shift in the position of the single emission band as a function of *x*. ESI-MS data also provided strong evidence that metal ion exchange is thermodynamically favored when the host and impurity have similar covalent radii. Similar observations have been reported in Co^{2+} doped CdS and ZnS QDs, where dopants were incorporated during ZnS growth, but were excluded from growth of CdS and were readily removed from the surface by coordinating ligands.[11]

Reversible temperature dependence of the ^1H chemical shifts in the $(Cd_{1-x}Co_x)$-4 clusters is unique and related to changes in the dynamics of the exchange processes of the terminal and bridging benzenethiolates with Co^{2+} incorporation. The fast ligand interconversion rate is the primary reason for the

DOI: 10.1021/acs.inorgchem.5b00421
Inorg. Chem. 2015, 54, 5757−5767

increased rate of cation exchange for Cd-4 compared to Zn-4. The ability to spectroscopically probe dopant substitution and equilibrium dynamics of these tetrameric clusters provides a platform to extend this study of molecular clusters with distinct "core" and "surface" metal sites such as $[M_{10}S_4(SPh)_{16}]^{4-}$ and $[M_{17}S_4(SPh)_{28}]^{2-}$ (M = Zn, Cd),[60,61] which is currently underway.

■ ASSOCIATED CONTENT

Supporting Information

Additional mass spectral figures and tables, NMR spectra, absorption spectra, ICP-OES data, and molecular orbital diagrams. The Supporting Information is available free of charge on the ACS Publications website at DOI: 10.1021/acs.inorgchem.5b00421.

■ AUTHOR INFORMATION

Corresponding Author

*E-mail: kittilstved@chem.umass.edu.

Notes

The authors declare no competing financial interest.

■ ACKNOWLEDGMENTS

This work was supported by start-up funds from the University of Massachusetts. Professors Michael Maroney, Paul Lahti, and Patricia Bianconi are acknowledged for fruitful discussions regarding the NMR results. We also thank M. Maroney for granting us access to the stopped-flow instrument. Mass spectral data were obtained at the University of Massachusetts Mass Spectrometry Center.

■ REFERENCES

(1) Kim, J. Y.; Voznyy, O.; Zhitomirsky, D.; Sargent, E. H. *Adv. Mater.* **2013**, *25*, 4986−5010.
(2) El-Sayed, M. A. *Acc. Chem. Res.* **2004**, *37*, 326−333.
(3) Steigerwald, M. L.; Brus, L. E. *Acc. Chem. Res.* **1990**, *23*, 183−188.
(4) Furdyna, J. K. *J. Appl. Phys.* **1988**, *64*, R29−R64.
(5) Beaulac, R.; Ochsenbein, S. T.; Gamelin, D. R. In *Colloidal Transition-Metal-Doped Quantum Dots*, 2nd ed.; Klimov, V. I., Ed.; CRC Press: Boca Raton, FL, USA, 2010; Chapter 11.
(6) Norberg, N. S.; Parks, G. L.; Salley, G. M.; Gamelin, D. R. *J. Am. Chem. Soc.* **2006**, *128*, 13195−13203.
(7) Nag, A.; Chakraborty, S.; Sarma, D. D. *J. Am. Chem. Soc.* **2008**, *130*, 10605−10611.
(8) Mocatta, D.; Cohen, G.; Schattner, J.; Millo, O.; Rabani, E.; Banin, U. *Science* **2011**, *332*, 77−81.
(9) Srivastava, B. B.; Jana, S.; Pradhan, N. *J. Am. Chem. Soc.* **2011**, *133*, 1007−1015.
(10) Hanif, K. M.; Meulenberg, R. W.; Strouse, G. F. *J. Am. Chem. Soc.* **2002**, *124*, 11495−11502.
(11) Radovanovic, P. V.; Gamelin, D. R. *J. Am. Chem. Soc.* **2001**, *123*, 12207−12214.
(12) Acharya, S.; Sarma, D. D.; Jana, N. R.; Pradhan, N. *J. Phys. Chem. Lett.* **2010**, *1*, 485−488.
(13) Archer, P. I.; Santangelo, S. A.; Gamelin, D. R. *Nano Lett.* **2007**, *7*, 1037−1043.
(14) Cumberland, S. L.; Hanif, K. M.; Javier, A.; Khitrov, G. A.; Strouse, G. F.; Woessner, S. M.; Yun, C. S. *Chem. Mater.* **2002**, *14*, 1576−1584.
(15) Archer, P. I.; Santangelo, S. A.; Gamelin, D. R. *J. Am. Chem. Soc.* **2007**, *129*, 9808−9818.
(16) Dalpian, G.; Chelikowsky, J. *Phys. Rev. Lett.* **2008**, *100*, 179703.
(17) Dalpian, G.; Chelikowsky, J. *Phys. Rev. Lett.* **2006**, *96*, 226802.
(18) Du, M. H.; Erwin, S.; Efros, A.; Norris, D. *Phys. Rev. Lett.* **2008**, *100*, 179702.
(19) Erwin, S. C.; Zu, L.; Haftel, M. I.; Efros, A. L.; Kennedy, T. A.; Norris, D. J. *Nature* **2005**, *436*, 91−94.
(20) Beaulac, R.; Archer, P. I.; Ochsenbein, S. T.; Gamelin, D. R. *Adv. Funct. Mater.* **2008**, *18*, 3873−3891.
(21) Du, M. H.; Erwin, S. C.; Efros, A. L. *Nano Lett.* **2008**, *8*, 2878−2882.
(22) Yu, J. H.; Liu, X. Y.; Kweon, K. E.; Joo, J.; Park, J.; Ko, K. T.; Lee, D.; Shen, S. P.; Tivakornsasithorn, K.; Son, J. S.; Park, J. H.; Kim, Y. W.; Hwang, G. S.; Dobrowolska, M.; Furdyna, J. K.; Hyeon, T. *Nat. Mater.* **2010**, *9*, 47−53.
(23) Eilers, J.; Groeneveld, E.; de Mello Donegá, C.; Meijerink, A. *J. Phys. Chem. Lett.* **2012**, 1663−1667.
(24) Beberwyck, B. J.; Surendranath, Y.; Alivisatos, A. P. *J. Phys. Chem. C* **2013**, *117*, 19759−19770.
(25) Rivest, J. B.; Jain, P. K. *Chem. Soc. Rev.* **2013**, *42*, 89−96.
(26) Son, D. H.; Hughes, S. M.; Yin, Y.; Alivisatos, A. P. *Science* **2004**, *306*, 1009−1012.
(27) Sahu, A.; Kang, M. S.; Kompch, A.; Notthoff, C.; Wills, A. W.; Deng, D.; Winterer, M.; Frisbie, C. D.; Norris, D. J. *Nano Lett.* **2012**, *12*, 2587−2594.
(28) Hencher, J. L.; Khan, M.; Said, F. F.; Tuck, D. G. *Inorg. Nucl. Chem. Lett.* **1981**, *17*, 287−290.
(29) Dance, I. G.; Choy, A.; Scudder, M. L. *J. Am. Chem. Soc.* **1984**, *106*, 6285−6295.
(30) Hagen, K. S.; Stephan, D. W.; Holm, R. H. *Inorg. Chem.* **1982**, *21*, 3928−3936.
(31) Türk, T.; Vogler, A.; Fox, M. A. *Adv. Chem.* **1993**, *238*, 233−241.
(32) Holah, D. G.; Coucouvanis, D. *J. Am. Chem. Soc.* **1975**, *97*, 6917−6919.
(33) Swenson, D.; Baenziger, N. C.; Coucouvanis, D. *J. Am. Chem. Soc.* **1978**, *100*, 1932−1934.
(34) Beecher, A. N.; Yang, X.; Palmer, J. H.; LaGrassa, A. L.; Juhas, P.; Billinge, S. J.; Owen, J. S. *J. Am. Chem. Soc.* **2014**, *136*, 10645−10653.
(35) Teunis, M. B.; Dolai, S.; Sardar, R. *Langmuir* **2014**, *30*, 7851−7858.
(36) Zheng, N.; Bu, X.; Lu, H.; Zhang, Q.; Feng, P. *J. Am. Chem. Soc.* **2005**, *127*, 11963−11965.
(37) Zadrozny, J. M.; Long, J. R. *J. Am. Chem. Soc.* **2011**, *133*, 20732−20734.
(38) Zadrozny, J. M.; Telser, J.; Long, J. R. *Polyhedron* **2013**, *64*, 209−217.
(39) Fataftah, M. S.; Zadrozny, J. M.; Rogers, D. M.; Freedman, D. E. *Inorg. Chem.* **2014**, *53*, 10716−10721.
(40) Maganas, D.; Sottini, S.; Kyritsis, P.; Groenen, E. J.; Neese, F. *Inorg. Chem.* **2011**, *50*, 8741−8754.
(41) Dance, I. G. *J. Am. Chem. Soc.* **1979**, *101*, 6264−6273.
(42) Dance, I. G. *Inorg. Chem.* **1981**, *20*, 2155−2160.
(43) Türk, T.; Resch, U.; Fox, M. A.; Vogler, A. *Inorg. Chem.* **1992**, *31*, 1854−1857.
(44) Bertoncello, R.; Bettinelli, M.; Casarin, M.; Maccato, C.; Pandolfo, L.; Vittadini, A. *Inorg. Chem.* **1997**, *36*, 4707−4716.
(45) Türk, T.; Resch, U.; Fox, M. A.; Vogler, A. *J. Phys. Chem.* **1992**, *96*, 3818−3822.
(46) Liu, H.-J.; Hupp, J. T.; Ratner, M. A. *J. Phys. Chem.* **1996**, *100*, 12204−12213.
(47) Nakata, M.; Ueyama, N.; Nakamura, A.; Nozawa, T.; Hatano, M. *Inorg. Chem.* **1983**, *22*, 3028−3035.
(48) Lane, R. W.; Ibers, J. A.; Frankel, R. B.; Papaefthymiou, G. C.; Holm, R. H. *J. Am. Chem. Soc.* **1977**, *99*, 84−98.
(49) Gaumet, J. J.; Strouse, G. F. *J. Am. Soc. Mass. Spectrom.* **2000**, *11*, 338−344.
(50) Løver, T.; Henderson, W.; Bowmaker, G. A.; Seakins, J. M.; Cooney, R. P. *Inorg. Chem.* **1997**, *36*, 3711−3723.
(51) Autissier, V.; Henderson, R. A. *Inorg. Chem.* **2008**, *47*, 6393−6403.
(52) Dean, P. A. W.; Vittal, J. J. *Can. J. Chem.* **1988**, *66*, 2443−2451.
(53) Cui, Z.; Henderson, R. A. *Inorg. Chem.* **2002**, *41*, 4158−4166.

DOI: 10.1021/acs.inorgchem.5b00421
Inorg. Chem. 2015, 54, 5757−5767

(54) Holm, R. H.; Eaton, S. S. *Inorg. Chem.* **1971**, *10*, 1446−1452.
(55) The increased line widths of the *o*-H's are too broad to resolve additional peaks with increasing Co^{2+} content.
(56) Holm, R. H. In *Dynamic Nuclear Magnetic Resonance Spectroscopy*; Jackman, L. M., Cotton, F. A., Eds.; Academic Press: New York, 1975; Chapter 9.
(57) Shannon, R. D. *Acta Crystallogr.* **1976**, *A32*, 751−767.
(58) Sengar, R. S.; Nemykin, V. N.; Basu, P. *New J. Chem.* **2003**, *27*, 1115−1123.
(59) Hagen, K. S.; Holm, R. H. *Inorg. Chem.* **1983**, *22*, 3171−3174.
(60) Choy, A.; Craig, D.; Dance, I.; Scudder, M. *J. Chem. Soc., Chem. Commun.* **1982**, 1246−1247.
(61) Lee, G. S. H.; Craig, D. C.; Ma, I.; Scudder, M. L.; Bailey, T. D.; Dance, I. G. *J. Am. Chem. Soc.* **1988**, *110*, 4863−4864.

DOI: 10.1021/acs.inorgchem.5b00421
Inorg. Chem. 2015, 54, 5757−5767